

Extension of the Bissell–Johnson plasma-sheath model for application to fusion-relevant and general plasmas

L. Kos,¹ N. Jelić,² S. Kuhn,² and J. Duhovnik¹

¹*LECAD Laboratory, Faculty of Mechanical Engineering, University of Ljubljana, SI-1000 Ljubljana, Slovenia*

²*Association EURATOM-ÖAW, Institute for Theoretical Physics, University of Innsbruck, A-6020 Innsbruck, Austria*

(Received 20 May 2009; accepted 13 August 2009; published online 28 September 2009)

This article presents an approach to solving a special Fredholm-type integral equation of the first kind with a particular kernel containing a modified Bessel function for applications in plasma physics. From the physical point of view, the problem was defined by Bissell and Johnson (B&J) [Phys. Fluids **30**, 779 (1987)] as a task to find the potential profile and the ion velocity distribution function in a plane-parallel discharge with a Maxwellian ion source. The B&J model is a generalization of the well-known Tonks–Langmuir (T&L) [Phys. Rev. **34**, 876 (1929)] discharge model characterized by a “cold” ion source. Unlike the T&L model, which can be readily solved analytically, attempts to solve the B&J model with a “warm” ion source have been done only numerically. However, the validity of numerical solutions up to date remains constrained to a rather limited range of a crucial independent parameter of the B&J integral equation, which mathematically is the width of a Gaussian distribution and physically represents the ion temperature. It was solved only for moderately warm ion sources. This paper presents the exact numerical solution of the B&J model, which is valid without any restriction regarding the above-mentioned parameter. It is shown that the ion temperature is very different from the temperature of the ion source. The new results with high-temperature ion sources are not only of particular importance for understanding and describing the plasma-sheath boundary in fusion plasmas, but are of considerable interest for discharge problems in general. The eigenvalue of the problem, found analytically by Harrison and Thompson [Proc. Phys. Soc. **74**, 145 (1959)] for the particular case of a cold ion source, is here extended to arbitrary ion-source temperatures. © 2009 American Institute of Physics. [doi:10.1063/1.3223556]

I. INTRODUCTION

Integro-differential equations of the Fredholm type are of high interest to plasma physics. While in some special cases they can be solved analytically, they in general cannot be solved without employing computational means. There is no general rule for solving such equations even when using combined analytic-numerical methods and techniques. Instead, each particular case must be tackled by means of particular computational tools, which depend on the structure of the equation, and primarily so on the particular kernel of the integral. However, the kernels, which appear in particular physics problems, can be so complicated that even with fairly good analytic-numerical algorithms huge computational resources must be employed to obtain a satisfactory solution during a reasonable period of time. Within the framework of our research on parallel computing we have encountered a particular problem related to general and fusion-oriented plasmas, namely, the Tonks–Langmuir¹ problem of collisionless discharges extended to the scenario when the ions within the discharge region are created at each point with a finite temperature. The number of various particles with a spectrum of various velocities at some point of observation is mathematically described by the velocity distribution function (VDF), which is a result of “counting” all the

particles that are capable of “visiting” that place, and their velocities. The VDF at some point of observation should be either measured in a real experiment, obtained from numerical simulations, or calculated via a suitable analytic-numerical method. All of these alternative approaches are extremely demanding and, consequently, have been solved only under certain restrictions, which lead to a limited validity of the results.

Our work deals with the analytic-numerical solution of an integral equation with a special kernel emerging from the physical scenario modeled first by Bissell and Johnson (B&J) in 1987.² The essential parameter of their problem is the ion-source temperature emerging from the Maxwellian-shaped ion-source velocity distribution at the place of their creation, i.e., “birth.” Due to mathematical and numerical difficulties, B&J approximated their kernel by Carleman’s formula via the Chebyshev polynomial expansion and, consequently, the validity of their solution remained limited to a rather narrow range of ion-source temperatures. In 1988, soon after the work of B&J had been published, Scheuer and Emmert (S&E) (Ref. 3) found a better kernel approximation and in addition applied a different analytic-numerical method for solving the B&J model. With the new kernel approximation, S&E extended the range of validity of the solution to

small ion-source temperatures, but for high ones the solution was still missing. Although the S&E extension of the solution to small ion-source temperatures was a considerable improvement from the analytic-numerical point of view, it attracted scarce academic attention for a number of years, primarily because the real problem of interest remained to solve the B&J problem for arbitrarily *high* ion-source temperatures (also applicable to, e.g., fusion plasmas) and not to just reproduce the Tonks and Langmuir (T&L) limit which was, indeed, well solved mathematically and interpreted physically. The use of currently available parallel-computing clusters now enables one to solve demanding integro-differential equations with much higher accuracy over a reasonable period of time, the only limitation being the accuracy of currently available software libraries. First, our work demonstrates such utilization of computer resources. Second, we present important new results related to the Bissell–Johnson model, namely: (i) we solve it with the *exact* kernel instead of using an approximate one, (ii) our solution is valid for an unlimited range of ion-source temperatures, and (iii) the accuracy of the solution is substantially increased by employing a high-density nonuniform computational grid with extremely high refinement near the boundaries of the computational region.

In addition, we obtain the ion VDF at any arbitrary point of the plane-parallel discharge, which enables us to calculate its moments (density, temperature, and higher-order moments) with special attention to the edge of the system, where boundary conditions for a discharge require a high degree of accuracy. From a practical point of view, this is especially important in applications to the scrape-off-layer (SOL) region near divertors in tokamak devices (see, e.g., Ref. 4). For the basic plasma physics determining the plasma boundary for arbitrary ion-source temperatures in the plasma approximation (i.e., assuming strict quasineutrality), it is, however, of crucial importance for further development of the intermediate region, which matches the sheath and plasma solutions obtained in asymptotic two-scale approximation (see, e.g., Ref. 5 and references therein). In fact, for the intermediate-scale approach the plasma approximation *cannot* be obtained by an alternative method such as particle-in-cell (PIC) simulations, where the simulation domain includes the physical boundary, i.e., an inherently unresolved plasma-sheath boundary. For such purposes, “idealization” of strict quasineutrality via the B&J or similar models is still of high interest.

Section II is a short reminder on the theoretical background of the existing theoretical and numerical methods with a description of upgrades applied in the present work. In Sec. III we present the results obtained via our approach. These results are summarized and discussed in Sec. IV where, in addition, the strategy for further development toward a complete plasma and sheath problem. The details of the theoretical and analytic-numerical method employed are given in the Appendices.

II. THEORETICAL BACKGROUND

A. General considerations

The general formulation of the problem as defined by T&L in 1929¹ for plane-parallel geometry consists in simultaneously solving Boltzmann’s equation for the ion VDF, $f_i(x, v)$,

$$v \frac{\partial f_i}{\partial x} - \frac{e}{m_i} \frac{d\Phi}{dx} \frac{\partial f_i}{\partial v} = S_i(x, v), \quad (1)$$

(where the collisional source term $S_i(x, v)$ on the right-hand side is a function reflecting the relevant microscopic physics involved in the model of interest, with x the Cartesian space coordinate, v the particle velocity, e the positive elementary charge, m_i the ion mass, and $\Phi(x)$ the electrostatic potential at position x), and Poisson’s equation for the potential,

$$-\frac{d^2\Phi}{dx^2} = \frac{e}{\epsilon_0} (n_i - n_e), \quad (2)$$

where ϵ_0 is the vacuum dielectric constant and $n_{i,e}$ are the ion and electron densities, respectively, with additional assumptions and proper boundary conditions imposed as described in Appendix A. In particular, T&L recognized that the problem can be split into and solved separately in the region where strict electric quasineutrality, $n_i - n_e = 0$, may be assumed (plasma or presheath region), and the region where quasineutrality is largely violated and a strong electric field occurs (the sheath region).

At this point we introduce the normalized quantities of interest as follows:

$$\begin{aligned} \frac{e\Phi}{kT_e} &\rightarrow \Phi, & \frac{m_i v^2}{2kT_e} &\rightarrow v^2, & \frac{x}{L} &\rightarrow x, & \frac{n_{i,e}}{n_{e0}} &\rightarrow n_{i,e}, \\ \frac{T_n}{T_e} &\rightarrow T_n, & \frac{T_{i,\text{src}}}{T_e} &\rightarrow T_{i,\text{src}}, & \frac{T_i}{T_e} &\rightarrow T_i, \\ \frac{\sqrt{2} c_{s0} f_i}{n_{e0}} &\rightarrow f_i, & S_i L &\rightarrow S_i, \end{aligned} \quad (3)$$

where $c_{s0} \equiv \sqrt{kT_e/m_i}$ and L is any characteristic length of the system, (usually, the half-length of the plane-parallel discharge). Let us note that in the articles by B&J and S&E both normalized quantities T_i and $\tau \equiv 1/T_i$ are used in parallel, while we prefer to avoid τ wherever possible. Moreover, in our notation T_n is the neutral temperature, which is identical to the ion-source temperature $T_{i,\text{src}}$. In the work of B&J this temperature was denoted as T_i leading to serious confusion. In fact, the final ion VDF turns out to be very different from the initial one. As an obvious example of such confusion, B&J defined in their work [Eq. (8)] the ion-sound velocity containing in fact the neutral temperature instead of the real (effective) ion temperature as should be calculated from the ion velocity distribution. So their Eq. (8) turns out to be nonsense emerging from confusion notation only. To avoid such problems we use the notation $T_{i,\text{src}} \equiv T_n$ for the ion source temperature, and T_i will be *exclusively reserved* for the final effective ion temperature as calculated from the final VDF.

Throughout the text we will use either non-normalized or normalized quantities. To avoid any possible confusion we will state explicitly in each case which of them is used in a given context. Additional normalized quantities will appear later in a natural way, but at this point we use the above ones for the purpose of rewriting Eqs. (1) and (2) in the normalized forms

$$\frac{\partial f_i}{\partial x} - \frac{d\Phi}{dx} \frac{\partial f_i}{\partial v^2} = \frac{S_i(x,v)}{v}, \quad (4)$$

$$-\varepsilon^2 \frac{d^2\Phi}{dx^2} = n_i - n_e, \quad (5)$$

respectively. Here,

$$\varepsilon \equiv \lambda_D/L \quad (6)$$

is the Debye length $\lambda_D = \sqrt{\varepsilon_0 k T_e / n_{e0} e^2}$, where n_{e0} is the electron density at the center of the plasma. The approximation $\varepsilon \rightarrow 0$ is called the ‘‘asymptotic two-scale limit,’’ which was first elaborated in a mathematically rigorous manner by Caruso and Cavaliere in 1962.⁶ Equation (5) shows that for $\varepsilon \rightarrow 0$ the quasineutrality condition holds, describing the plasma or presheath region with an infinitely thin sheath manifesting itself by the ‘‘sheath singularity.’’ If, on the other hand, the ‘‘sheath scaling’’ $x/\lambda_D \rightarrow x$ is employed, the sheath becomes infinitely wide. T&L simply started from the quasineutrality condition and simplified the problem further by assuming that all ions are born with zero velocity (‘‘cold’’ or ‘‘singular’’ ion-source velocity distribution). Furthermore, they assumed that the discharge is symmetric about the center [position $x=0$, with $\Phi(0)=0$ as illustrated in Appendix A]. In addition, the floating-wall condition (i.e., the equality of electron and ion fluxes at both sides of the discharge) is imposed, with the assumption that the electron density is Boltzmann-distributed:

$$n_e = n_{e0} \exp\left(\frac{e\Phi}{kT_e}\right), \quad (7)$$

where T_e is the electron temperature. In any case, the above normalization is an arbitrary one. This is because the length (or half length) of the system L can be renormalized depending on particular needs, (e.g., to the ionization length for applying intermediate-scale theory). Following B&J and the subsequent work of S&E, we temporarily disregard alternative possibilities and proceed to work in non-normalized notation. The general formal solution of Eq. (1) can be found by integrating Eq. (1) along the characteristics of the kinetic equation, which are identical with the collisionless particle trajectories and satisfy the differential equation

$$\frac{dv}{dx} = -\frac{e}{m_i} \frac{d\Phi}{dx} \frac{1}{v}, \quad (8)$$

with which Eq. (1) transforms into

$$\frac{df_i}{dx} = \frac{S_i}{v}. \quad (9)$$

Upon integrating Eq. (8), the characteristic passing through the point (x,v) can be expressed in the form

$$v' = \text{sgn}(v') \sqrt{v^2 + \frac{2e}{m_i}(\Phi - \Phi')}, \quad (10)$$

where (x',v') is any generic point on the characteristic, $\Phi' = \Phi(x')$, and $\Phi = \Phi(x)$. Integrating Eq. (9) along the characteristic (10) from $(x'_{\text{in}}, v'_{\text{in}})$ (its point of entrance into the system) to the point (x,v) , the formal solution is found in the form

$$f_i(x,v) = f'_{i,\text{in}} + \oint_{x'_{\text{in}}}^x \frac{dx'}{v'} S', \quad (11)$$

where $f'_{i,\text{in}} = f_i(x'_{\text{in}}, v'_{\text{in}})$, $S'_i = S_i(x', v')$, $= S(x', \text{sgn}(v') \sqrt{v^2 - 2e[\Phi(x') - \Phi(x)]/m_i})$, and \oint indicate that the integration is carried out along the characteristic. In the present context, $f'_{i,\text{in}} = 0$ because we assume that no ions come from the walls. The ion density is an integral of the ion velocity distribution over velocity

$$\begin{aligned} n_i(\Phi) &= \int_{-\infty}^{+\infty} f_i(x,v) dv \\ &= \sum_I \int_{-\infty}^{+\infty} dv \\ &\quad \times \oint_{x'_{\text{in}}}^x \frac{S_i\left(x', \text{sgn}(v') \sqrt{v^2 - \frac{2e}{m_i}(\Phi' - \Phi)}\right)}{\text{sgn}(v') \sqrt{v^2 - \frac{2e}{m_i}(\Phi' - \Phi)}} dx', \end{aligned} \quad (12)$$

where summation over I takes into account various ion populations reaching the observation point either from the left or right the right-hand side. The particular method of trajectories used in this work for obtaining all the ion populations contributing to the total ion velocity distribution is elaborated in Appendix B.

B. Bissell and Johnson’s original solution

While T&L solved the problem with a ‘‘cold’’ (singular) ion source via an expansion method, Harrison and Thompson (H&T) (Ref. 7) in 1962 found the exact solution for the singular ion source. B&J, however, supposed that the ion-source distribution is also Maxwellian, i.e., *regular* in the sense of the finite ion source temperature $T_n \equiv T_{i,\text{src}}$

$$S(x,v) = R n_n n_e \sqrt{\frac{m_i}{2\pi k T_n}} \exp\left(-\frac{m_i v^2}{2k T_n}\right), \quad (13)$$

where R is ionization rate as denoted by B&J and n_n is the neutral gas density (which is assumed to homogeneous over the discharge). The particular scenario of B&J, assuming a Maxwellian ion source with the ionization rate proportional to the electron density, is elaborated in detail in Appendix A.

In their original work, B&J performed the integration over velocity space and interchanged the independent and dependent variables using the identity

$$dx' \equiv \frac{dx'}{d\Phi'} d\Phi' \equiv \Psi d\Phi', \quad (14)$$

so that Eq. (A8) from Appendix A takes the form

$$\frac{1}{B} = \int_0^{\Phi_b} \Psi(\Phi') \exp \left[\left(1 + \frac{1}{2T_n} \right) (\Phi - \Phi') \right] \times K_0 \left(\left| \frac{\Phi - \Phi'}{2T_n} \right| \right) d\Phi', \quad (15)$$

with

$$\Psi(\Phi') = \frac{dx'}{d\Phi'} \quad \text{and} \quad x(\Phi_b) = 1. \quad (16)$$

The details on obtaining Eq. (15) are given in Appendix B. B&J used a switch function

$$J(\Phi' - \Phi) = \exp[\tau(\Phi' - \Phi)] \{ 1 - \tanh[(\Phi' - \Phi)/\epsilon] \} / 2 + \{ 1 + \tanh[(\Phi' - \Phi)/\epsilon] \} / 2, \quad (17)$$

which led to their main equation

$$\frac{1}{B} = \int_0^{\Phi_b} d\Phi' \Psi(\Phi') F(\Phi' - \Phi), \quad (18)$$

with the kernel

$$F(\theta) = J(\theta) \exp(\theta) \exp\left(\frac{\tau}{2}|\theta|\right) K_0\left(\frac{\tau}{2}|\theta|\right). \quad (19)$$

They applied a complicated mathematical procedure assuming an approximation of such a kernel via a Chebyshev polynomial series, yielding a system of linear equations. They claimed that their approximation is more or less valid in the narrow range of T_n between 0.5 and 4. We repeated their derivations and in Fig. 1 we plot their kernel approximation with our corresponding results where we have taken into account that there were certain mistakes in the polynomial coefficients given by B&J.

Carefully following the B&J approach, we calculated a closer approximation of the kernel. One can notice differences between the approximated and the exact kernel. The B&J approach is a specific one and the system of linear equations to be solved is closely related to the approximation they used. B&J concluded from the quantities derived that the approximation to the kernel of the plasma equation for $T_e/T_n > 2$ was too poor to be usable. However, the range of validity of the kernel is too narrow both for plasmas with small temperatures and plasmas with ion-source temperatures sufficiently high for fusion application.

C. The Scheuer and Emmert approach

S&E used the B&J equation in a different form, in which the kernel contains the unknown function. We express the basic relation of their approach as

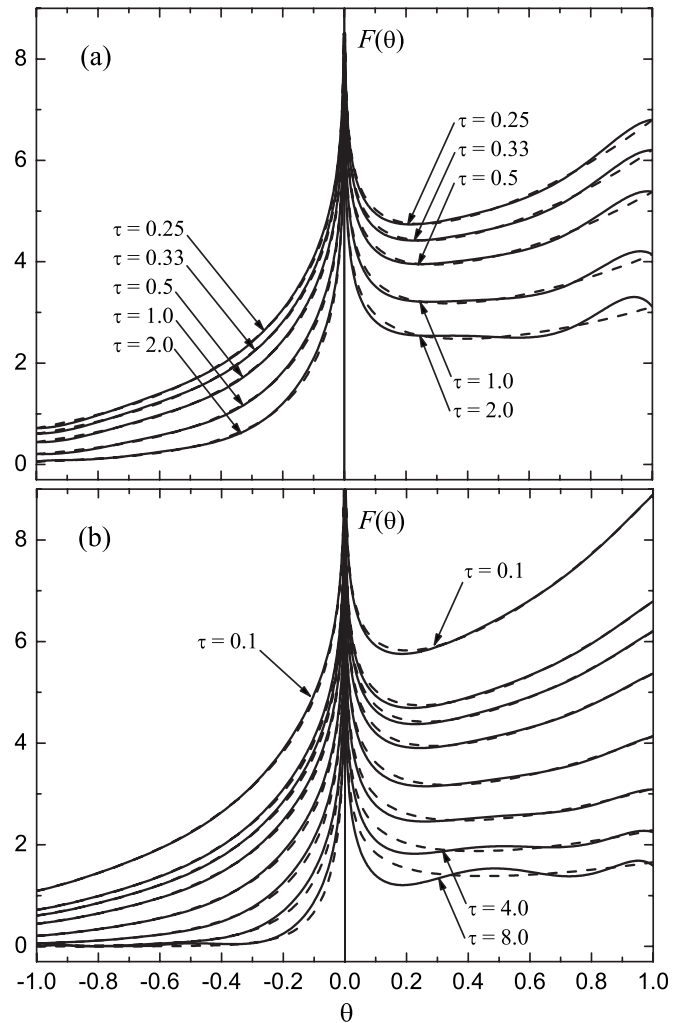


FIG. 1. Comparison of the approximated and exact kernel $F(\theta)$ of the B&J equation: (a) B&J approximation and (b) our approximation with the exact kernel (dashed) for various values of $\tau = T_e/T_n$. The error of the approximation increases with increasing τ 's. While our approximation is better near $\theta = \Phi' - \Phi = 1$, it is still evident that errors at the center are significant and cannot be lowered with a polynomial approximation of order eight.

$$\frac{1}{B} = \int_0^1 \exp \left[\left(1 + \frac{1}{2T_n} \right) (\Phi - \Phi') \right] K_0 \left(\left| \frac{\Phi - \Phi'}{2T_n} \right| \right) dx'. \quad (20)$$

This is a more universal approach, yet they also introduced an approximation of the kernel due to integration problems with the logarithmic singularity. They approximated K_0 with

$$K_0(|u|) = -\ln\left(\frac{|u|}{2}\right) \sum_{i=0}^6 b_i \left(\frac{|u|}{3.75}\right)^{2i} + \sum_{i=0}^6 a_i \left(\frac{|u|}{2}\right)^{2i} \quad (21)$$

and expanded the logarithmic term to get an analytic formula in piecewise linear zones. In addition, S&E employed a non-uniform grid near $x=1$. The polynomial approximation (21) from Ref. 8 is valid only for $u \leq 2$. The relative error in the range $[0,2]$ is under 10^{-7} , while for $u > 2$ another polynomial approximation, with a factor $e^{|u|}/\sqrt{|u|}$, is used that leads to difficulties in the analytical evaluation of the zones. Similar to B&J, kernel-approximation errors lead us to the conclu-

sion that present the approaches cannot be used for wide temperature ranges.

Nevertheless, the S&E approach turns out to be perfectly suited for both our and future numerical investigations. In fact, unlike the purely analytic method by H&T, the subsequent analytic-numerical method by Riemann (see, e.g., Ref. 5), and the B&J numerical method, *where the electric field is the main quantity of interest*, the S&E method is based on finding the *potential profile* without interchanging dependent and independent variables. This method is a fairly universal one appearing suitable for solving numerically a wide class of integro-differential equations, which could not be classified as Fredholm ones (and probably could not be classified at all-e.g., as Hammerstein ones, as we will see for the finite- ε case). Following the S&E approach, we proceed our numerical investigations with our own refinements as follows.

D. Our numerical approach applied

In our work we basically follow the approach adopted by S&E. However we have improved it by (i) using the exact kernel, (ii) applying a much better resolution of the computational grid, and (iii) employing high grid refinements at both the zero and the infinite-electric-field sides of the discharge.

Following the “trick” applied by S&E, we introduce the identity

$$1/B \equiv \exp(\phi_0), \quad (22)$$

so Eq. (20) takes the form

$$\begin{aligned} \exp(\phi_0) &= \int_0^1 \exp\left[\left(1 + \frac{1}{2T_n}\right)(\phi - \phi')\right] \\ &\times K_0\left(\left|\frac{\phi - \phi'}{2T_n}\right|\right) dx', \end{aligned} \quad (23)$$

where the simple formal identity $\phi - \phi' = \Phi - \Phi' = (\Phi - \phi_0) - (\Phi' - \phi_0)$ has been introduced. Equation (20) can be rewritten into

$$\begin{aligned} &\exp\left[-\left(1 + \frac{1}{2T_n}\right)\phi\right] \\ &= \exp(-\phi_0) \times \int_0^1 \exp\left[-\left(1 + \frac{1}{2T_n}\right)\phi'\right] \\ &\times K_0\left(\left|\frac{\phi - \phi'}{2T_n}\right|\right) dx \end{aligned} \quad (24)$$

or, after taking the logarithms of both sides, into a form suitable for numerical processing,

$$\begin{aligned} \left(1 + \frac{1}{2T_n}\right)\phi &= \phi_0 - \ln\left[\int_0^1 \exp\left[-\left(1 + \frac{1}{2T_n}\right)\phi'\right] \right. \\ &\times K_0\left(\left|\frac{\phi - \phi'}{2T_n}\right|\right) dx' \Bigg], \end{aligned} \quad (25)$$

with $K_0(z)$ the zeroth-order modified Bessel function of the second kind, which is singular at every $x' = x$. The unknown

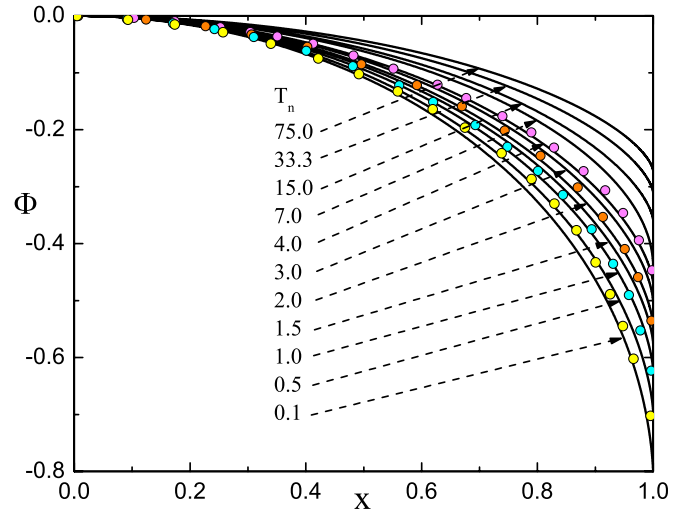


FIG. 2. (Color online) Potential profiles for various ion-source temperatures as obtained by us with the exact kernel (solid lines) and by B&J with their approximate kernel (scattered).

function of interest, $\phi(x)$, which is integrated over the normalized unit interval, also includes a known high gradient at $x=1$, while at $x=0$, due to symmetry, it is expected to have a zero gradient.

Details on the numerical method applied and implementation aspects are given in Appendix C.

III. RESULTS

The Fredholm equation with the B&J kernel has a solution for the electric potential lying between the analytic value of the Tonks–Langmuir limit ($\Phi > \Phi_s = -0.854$ at the sheath entrance) and zero (at the center plane of symmetry). The particular value of Φ_s depends on the ion-source temperature. In Fig. 2 we show the potential profiles as calculated in a wide range of ion temperatures (solid lines) in contrast to B&J (scattered). It can be seen that both sets of B&J and our results closely overlap in the range of temperatures where B&J obtained results. There is, however, a small discrepancy for $T_n = \{0.5, 1, 2, 4\}$, which may be ascribed to B&J errors in the kernel as we demonstrated in Fig. 1. There is an additional error in the presentation of B&J results in Fig. 2, which originates from the fact that we did not have their exact data available but used scanned data from Fig. 4 from their article² instead. This issue, however, is not of primary importance to the present work, since we are interested in the method without approximation. Our next step is to compare our results for the electric potential with those obtained with a more reliable kernel as employed by S&E. We do not show a comparison of our potential profiles with S&E results since they presented one single curve, i.e., for $T_i = 1$. In addition, the shape of their single curve differs from our results and thus also from those of B&J. Our other investigations (to be published) performed via the PIC simulation^{9,10} (in particular with BIT1¹¹) have shown that the S&E curve perfectly fits the case with a uniform ion source rather than with one proportional to the electron density. It seems that, in fact, S&E by

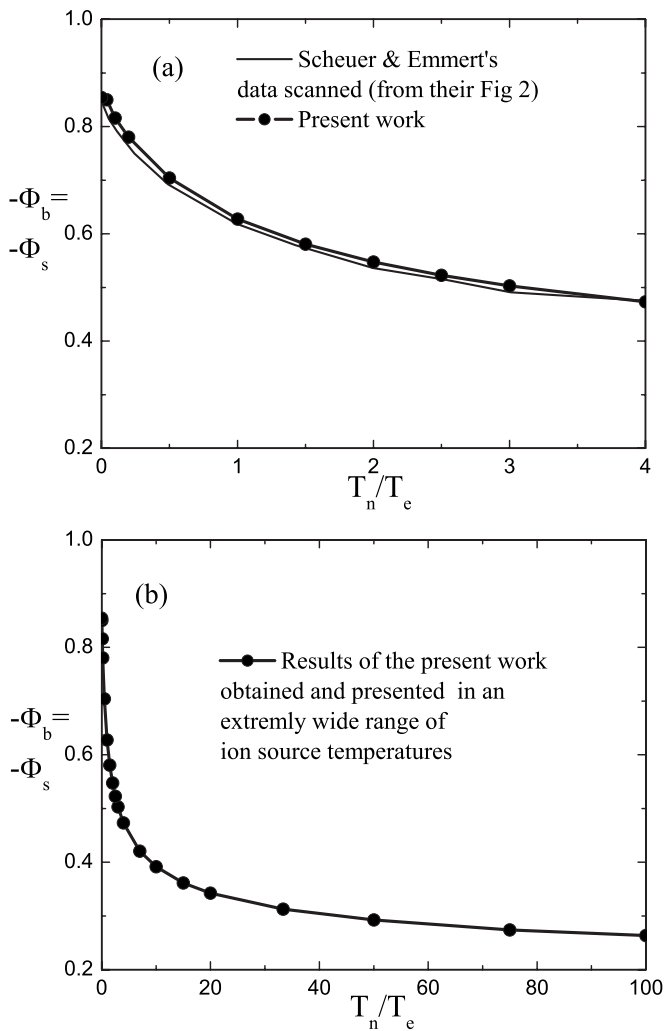


FIG. 3. The plasma sheath boundary potential in a limited range of ion source temperatures, where the S&E approximate kernel is valid, in comparison with our results (a), and in a wide range of the ion source temperatures (b), where we employed the exact kernel.

mistake presented an actually excellent result, but probably obtained for a different discharge scenario.

The dependence of the potential Φ_s at the quasineutral plasma (presheath) boundary on the ion source temperature is shown in Fig. 3. The end or breaking point of the solution, i.e., the plasma boundary Φ_s , corresponds to the place where the electric field becomes infinite. In Fig. 3(a) we show the dependence of the breaking point in a “zoomed” range where the S&E results are taken from their article. It is clear that our results overlap with the S&E results. The small discrepancy can be ascribed to the fact that our method is a very advanced one, i.e., based on at least 1600 cells (whereas S&E used 100 cells) and that we used the exact kernel instead of their approximate one. Our solution in an extremely wide range of ion source temperatures is shown in Fig. 3(b).

Once the potential profile is known, it determines the actual velocity distribution at the observation point, provided the source velocity distribution is exactly specified, as is the case with the B&J model and the present investigation. Figure 4 illustrates our velocity distributions for the cases of a small and moderately high ion source temperatures in com-

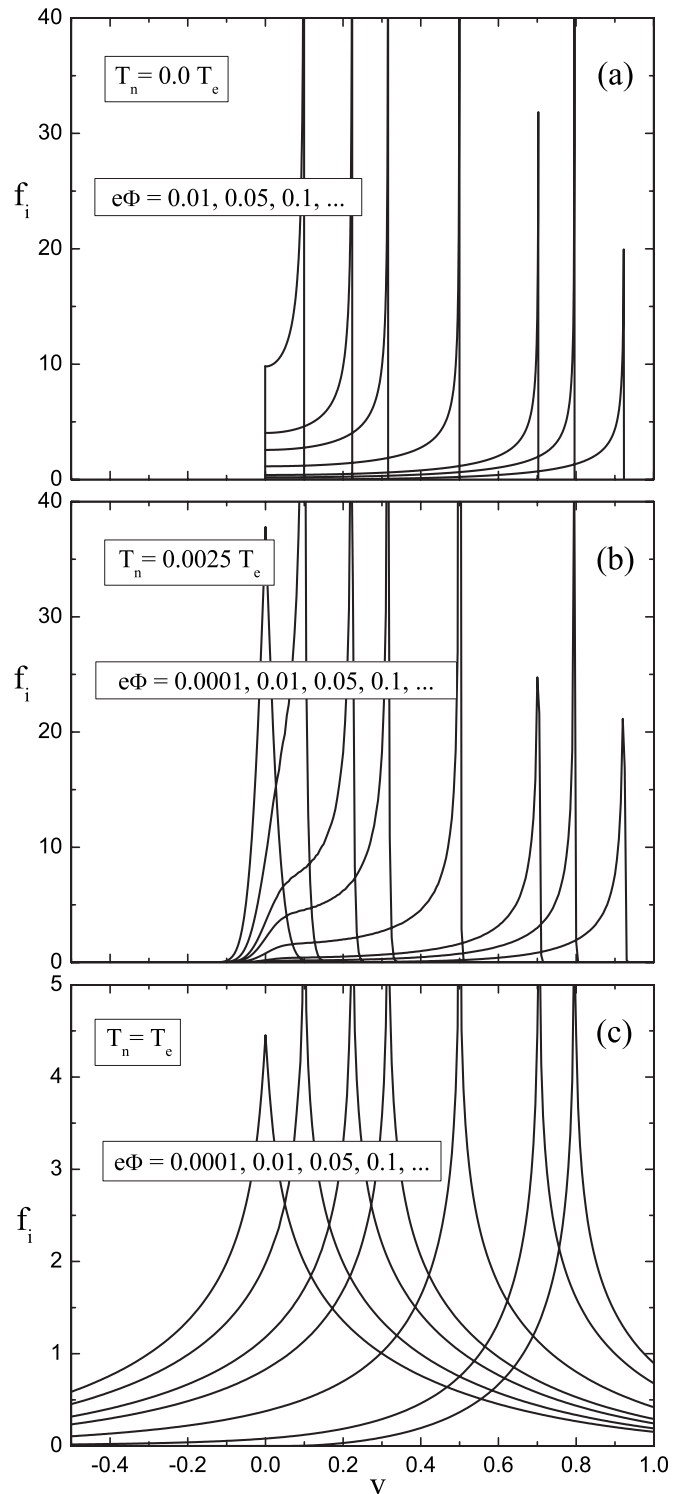


FIG. 4. Analytic velocity distribution of T&L in the case of the zero-ion-temperature source in comparison with our results with a finite ion temperature source.

parison with the cold-ion-source case (T&L). It is seen that for small ion source temperatures the shape of the velocity distribution resembles the T&L limit, while with higher ion source temperatures it resembles the S&E results.

Once the ion velocity distribution as a function of position (or equivalently, of the potential corresponding to the latter) has been found, one can calculate from it fluid quan-

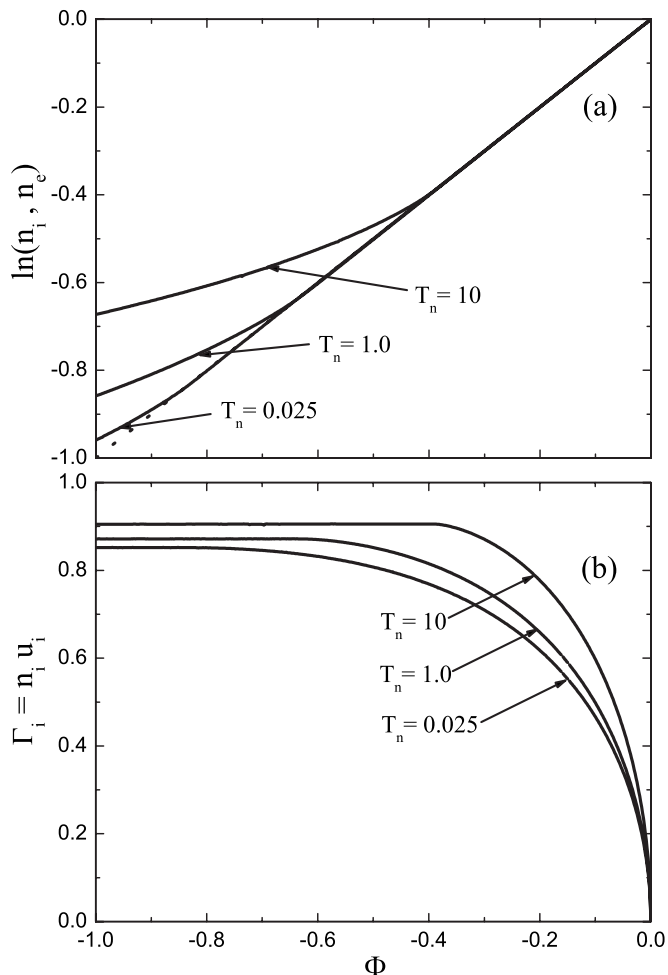


FIG. 5. (a) Ion and electron densities in a logarithmic presentation as a function of local potential $\Phi(x)$. (b) Ion flux as a function of $\Phi(x)$.

ties such as density, particle flux, total energy flux, temperature, and higher moments of velocity distribution such as heat flux, etc., as described in Appendix B. While B&J made a step forward by analytically preparing the integrals of the moments of the VDF for faster numerical calculation, S&E (Ref. 3) performed direct numerical calculation using some kind of “brute force.” The latter is a more expensive yet more universal method, which is applicable to arbitrary analytic and experimental velocity distributions, so we prefer to apply it in our present and future work. In Fig. 5(a) we illustrate the ion density profiles in a logarithmic presentation for three particular temperatures (solid lines) in comparison with the electron density, which, by the definition of the model, is Boltzmann-shaped. As expected, the ion densities follow the straight line in the region of quasineutrality and more or less sharply change such behavior at the positions of the field singularity (plasma boundary).

In Fig. 5(b) we show the corresponding dimensionless ion fluxes [defined by Eq. (B7)], also calculated directly from the ion velocity distribution. The ion flux is seen to increase in the plasma region but to become practically independent of the sheath potential to the left of the plasma boundary. In the sheath region, however, relevant assump-

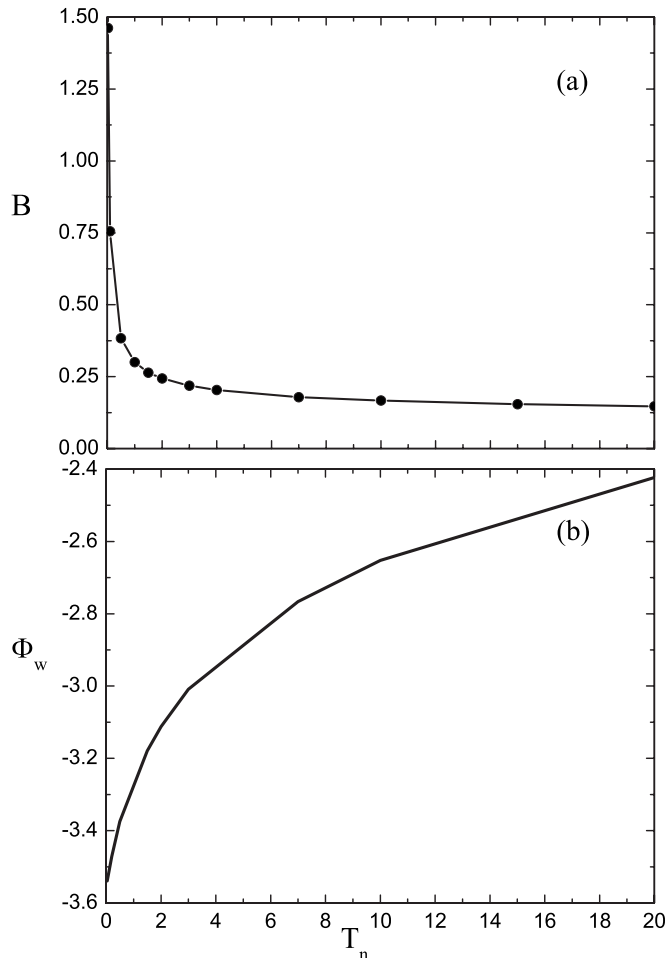


FIG. 6. The dependence of B (a) and of the wall potential (b) on the ion source temperature.

tions of the model become invalid, so they should be ignored.

As pointed out in Appendix C, the quantity B is calculated from equality Eq. (C9) iteratively in a numerical procedure. With the density calculated from the velocity distribution, it turns out *a posteriori* that the product Bn_i is constant, i.e., with a high degree of accuracy equals unity. The result of calculating B as a function of the source temperature at an arbitrary point (e.g., near the center of the system) is illustrated in Fig. 6(a).

The next step is to calculate the normalized average plasma density over the system from $\int_0^1 n_e[\phi(s)] ds$, and based on this, to calculate the wall potential with known B . The result is shown in Fig. 6(b) for a wide range of ion source temperatures. These results tally well with those of B&J; however, our results are not limited to the ion source (neutral) temperatures.

Figure 7 shows the effective ion (final) temperature T_i as a function of the local potential for various ion source temperatures T_n . The upper figure shows the distribution of the ion temperature in a wide range of ion source temperatures, while the bottom figure represents a “zoom” for a very cold ion source in comparison with a result obtained by using Riemann’s software¹² for the limit of the zero ion source temperature. It is evident that high ion source temperatures

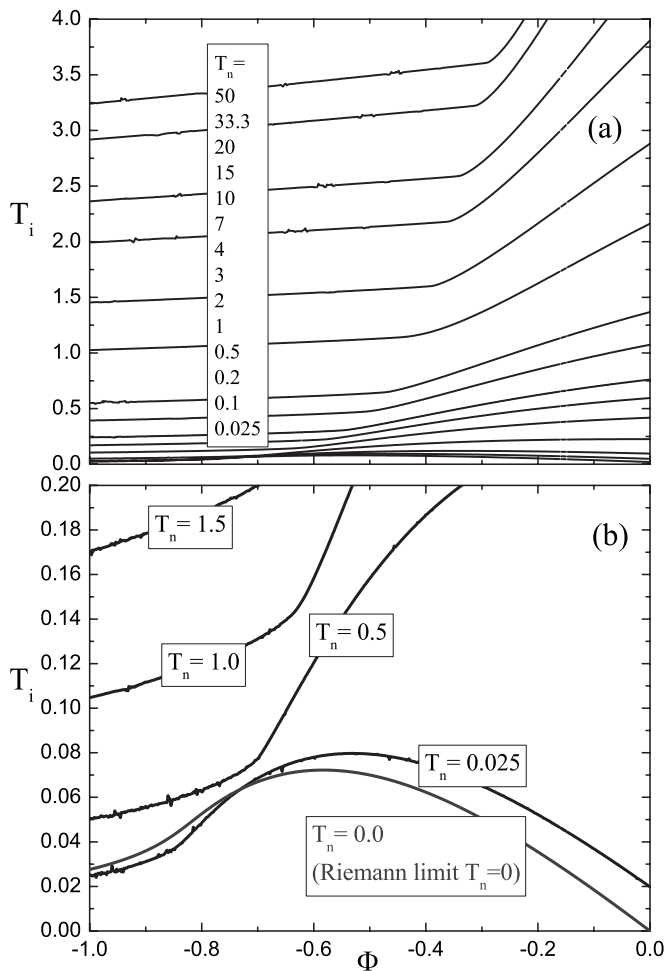


FIG. 7. Profiles of the ion temperature T_i [defined according to Eq. (B10)] for various ion source temperatures.

yield a final temperature, which is smaller by an order of magnitude. This fact is of high importance for both general plasma physics and for fusion investigations, where the ions from the core region penetrate the SOL region with rather high temperatures but their temperature might suddenly drop therein. For a better insight into this effect, Fig. 8 shows the dependence of the effective temperature both at the center of the discharge and at the plasma edge as a function of the ion source temperature. It is apparently strange that the final ion temperature is lower by almost an order of magnitude than the ion source temperature. This is a consequence of the ion “cooling” due to energy losses at the boundary. Our result on the final temperature T_i is in good agreement with the results given by B&J for several particular cases.

Some doubts may appear regarding the numerical calculation of the moments from the final velocity distribution due to its singular character. We resolve this dilemma via by comparing T_i as calculated with extreme precision via Riemann’s software and with our direct integration method. We used our own software (to be further elaborated in our next article, which will extend the present work to the case of finite temperature and finite ε), which is based on Eq. (27). In the example in Fig. 9 this software is applied to the case of an extremely small value of ε ($\varepsilon = 10^{-5}$) for an extremely

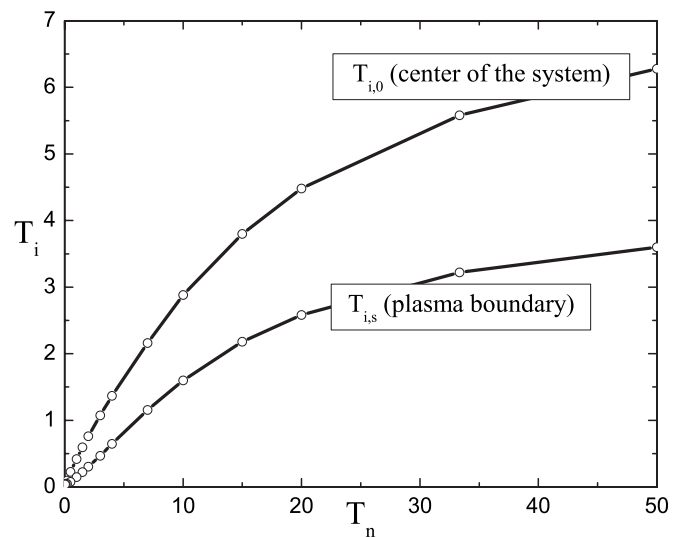


FIG. 8. Ion temperature at the center and the edge of the plasma for various ion source neutral temperatures.

small ion source temperature ($T_n = 0.002$). The temperature profiles obtained by means of these approaches are illustrated in Fig. 9.

Regarding the normalization lengths of the plasma, it should be noted that such various lengths can be defined in an arbitrary manner. In fact, it is clear from the condition $\int f(v)dv \equiv \int Cf(v)d(v/C) = 1$ that in the Boltzmann equation we can also use any normalization of the velocity distribution with an arbitrary constant C , as well as put any other normalized length x/ℓ , with ℓ an arbitrary constant length, instead of x/L . The “proper” normalization should be decided on the basis of further purposes. While the first normalized length (x/L) just corresponds to a calculation domain extending from 0 to 1, the second one (x/ℓ) is desired to be a physical quantity of interest for particular purposes. According to H&T (Ref. 7) and Self,¹³ the proper normaliza-

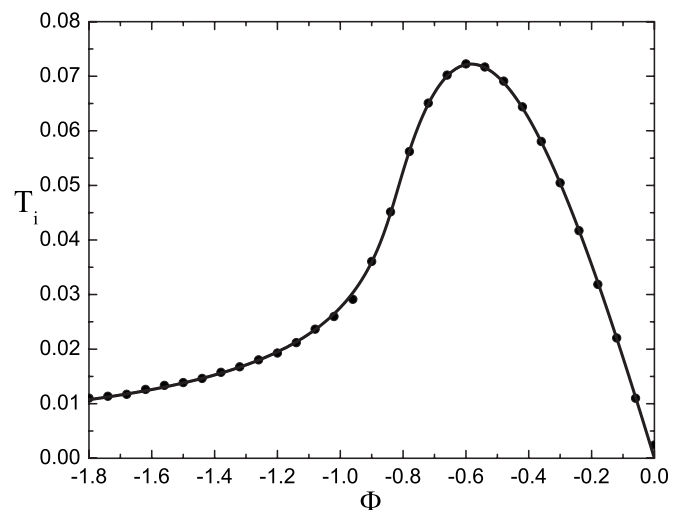


FIG. 9. Comparison of the results obtained via Riemann’s program (solid line) and ours obtained via the direct integration method used in the present work (scattered). For this comparison we used our software based on Eq. (27) applied to the case of an extremely small $\varepsilon = 10^{-5}$ for an extremely small ion source temperature ($T_n = 0.002$).

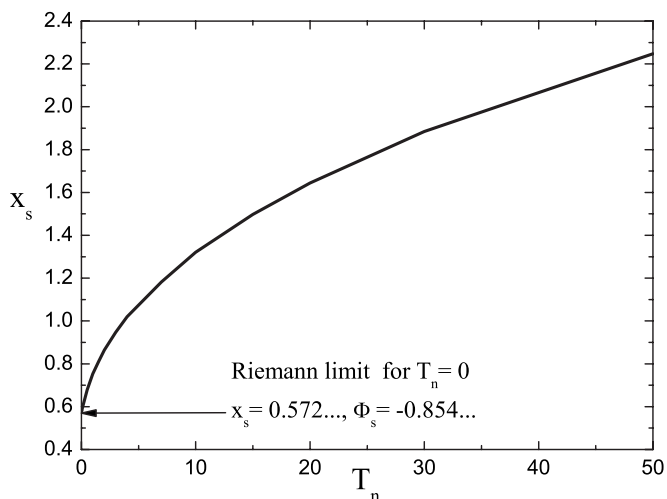


FIG. 10. Renormalized presheath length x_s as a function of the ion-source temperature.

tion in the limit of vanishing ion source temperature and vanishing ε is an analytic value that depends on the ionization mechanism and in the case of ionization proportional to the electron density yields the exact value $x_s=0.405\dots$ (plasma boundary, where electric field becomes singular). Riemann, however, prefers to use a slightly different normalization (see e.g., Ref. 5), which yields the said value multiplied by $\sqrt{2}$, i.e., $x_s=0.572\dots$ By comparison of the derivation of B&J with that of Riemann we found that the renormalization

$$\frac{x}{L} \rightarrow \frac{x}{\ell} \equiv B\sqrt{2\pi T_n} \quad (26)$$

(where T_n is normalized to T_e) is equivalent to rescaling the system to the ionization length ℓ . The result is shown in Fig. 10, however, not only for the “classical” case of vanishing ion source temperature but, instead, for arbitrary values thereof. Our “empirical” extension of the Harrison–Thompson result to an arbitrary ion source temperature is very important for application to the theory of the intermediate plasma-sheath region, which due to lack of any data on the ionization length in the case of the finite ion temperature up to now was limited to the “cold” ion source case only (see e.g., recent works by Riemann⁵).

After obtaining all desired quantities like the ion density and temperature, one is also capable to calculate other derived quantities. One such quantity, which has recently been introduced in plasma physics by Kuhn *et al.*¹⁴ and Jelić *et al.*¹⁵ is the “local polytropic coefficient,” which is of high importance to plasma sheath determination. In fact, for engineering purposes the definition of the plasma sheath boundary as the point where the ion-sound velocity equals the fluid ion velocity might be of considerable interest. However, determining the ion-sound velocity requires the knowledge of local “ion polytropic coefficient” γ . So far there has not been a reliable model to treat this quantity for the regular ion source temperature case. Our solution enables one to further investigate this issue in detail in the near future. Our Fig. 11 is just an illustration of the behavior of the polytropic coef-

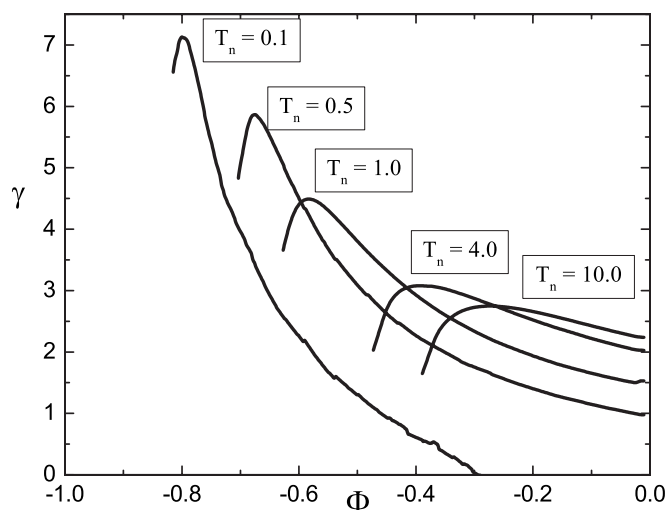


FIG. 11. Illustration of the local ion polytropic coefficient for several ion source temperatures.

ficient, which is important in local ion sound velocity calculations. It has been suggested by Kuhn *et al.*¹⁴ that the maximum of γ may be a possible means of defining the plasma-sheath boundary. Our Fig. 11 confirms that this “coincidence” still holds for low ion source temperatures (curve $T_n/T_e=0.1$). Apparently, the deviation from this rule becomes strong as the ion temperature increases.

IV. DISCUSSION AND CONCLUSION

In this work we have used S&E’s (Ref. 3) numerical approach to extended the B&J model² to arbitrary ion source temperatures. However, due to their approximation of the kernel, the S&E approach is still limited to plasmas with low ion temperatures. So we have employed an exact kernel and at the same time refined the approach of S&E, i.e., applied a high-density and a high-resolution grid. For confirmation of numerical stability and precision, our results were obtained in both MATHEMATICA and in our own package, yielding an excellent agreement in all numerical figures. From the physical point of view we found that the final ion temperature is much lower than the ion source temperature. This is quite important in fusion devices, where ions penetrate from the core to the SOL region and then, moving toward the divertor plate, become rapidly cooled. Most significantly, we found the plasma edge x_s as a function of the ion source temperature. Finally, we have shown that in finite-temperature plasmas the maximum of the polytropic coefficient in fact does not coincide with the edge of the plasma sheath as this is the rule in plasmas with negligible ion-source temperatures, but still can be considered as a good estimation of the plasma-sheath boundary. This fact might be of considerable importance to linking fluid and kinetic plasma parameters in fusion fluid codes like e.g., SOLPS-B2 (e.g., Ref. 16).

It should be pointed out that our results are strictly valid only up to the breaking point of the quasineutrality. For a solution which is valid for the whole system it would be necessary to involve the effect of the electric field, i.e., to

start from the full Poisson equation instead of using the quasineutrality condition. Such an approach leads to the integro-differential equation, which we have obtained in the form

$$\begin{aligned} \frac{1}{B} &= \frac{1}{1 - \exp(-\Phi)\varepsilon^2 \frac{d^2\Phi}{dx^2}} \\ &\times \int_0^1 \exp\left[\left(1 + \frac{1}{2T_n}(\Phi' - \Phi)\right)\right] \\ &\times K_0\left[\frac{1}{2T_n}|\Phi' - \Phi|\right] dx'. \end{aligned} \quad (27)$$

In order to solve this equation we are developing a new program package, so the results will soon be available. In view of future tasks, we have found here that the eigenvalue of the problem, which considerably overlaps with the classic value of H&T, can be further refined by more expensive calculation runs.

ACKNOWLEDGMENTS

This work was supported by the European Commission under (i) the Contract of Association between EURATOM and the Austrian Academy of Sciences, (ii) the Contract of Association between The European Atomic Energy Community (EURATOM) and the Ministry of Higher Education, Science and Technology of the Republic of Slovenia No. FU06-CT-2007-00065, and by (iii) the Austrian Science Fund (FWF) under Project No. P19333-N16. It was carried out within the framework of the European Fusion Development Agreement. The views and opinions expressed herein do not necessarily reflect those of the European Commission.

Numerical calculations associated with this work were supported by the Austrian Ministry of Science and Research (BMWF) as part of the UniInfrastrukturprogramm of the Forschungsplattform Scientific Computing at the Leopold-Franzens Universität (LFU) Innsbruck. The authors are indebted to K.-U. Riemann for his permanent advice and instructions on theoretical aspects, as well as for using his software in order to obtain the results in the limit of zero ion temperature. We are obliged to D. D. Tskhakaya Sr. for checking out the derivations of formulas and many valuable discussions on physical theoretical points.

APPENDIX A: B&J MODEL

Physically, the B&J model implies that the ions are created from single electron-neutral impact-ionization, i.e., the ionization rate is collisionless, proportional to the electron density. Other basic sources were elaborated by Self.¹³ With Maxwellian ions the T&L model appears to be a Dirac δ function as a limiting case of $\exp(-x^2/a^2)/a\sqrt{\pi}$, with $a \rightarrow 0$. With a Maxwellian source one can perform an integration over the velocity. The result is

$$\begin{aligned} n_i &= \sqrt{\frac{m_i}{2\pi kT_n}} R n_n n_e \times \sum_l \int \exp\left(1 + \frac{e(\Phi' - \Phi)}{2kT_n}\right) \\ &\times K_0\left(\left|\frac{e(\Phi' - \Phi)}{2kT_n}\right|\right) dx'. \end{aligned} \quad (A1)$$

The ion flux at the boundary obtained from the continuity equation $d\Gamma_i/dx = R n_n n_e$, which after integration takes the form

$$\Gamma_i = R n_n \int_0^L n_e dx \equiv L R n_n n_{e,av}, \quad (A2)$$

where $n_{e,av}$ is the mean value of the electron density over the system. The electron flux for Maxwellian distribution at a plasma-sheath boundary is approximately

$$\Gamma_e = \sqrt{\frac{kT_e}{2\pi m_e}} \exp\left(\frac{e\Phi_b}{kT_e}\right) n_0. \quad (A3)$$

The most ‘‘standard’’ assumption in collisionless discharge models that the ion and electron fluxes at the boundary are equal ($\Gamma_i = \Gamma_e$), so there is no electric current. In the present case, this ‘‘floating wall’’ condition yields $\Phi_b \equiv \Phi_w$ where w denotes the physical wall. Current balance so becomes

$$L R n_n = \frac{n_0}{n_{e,av}} \sqrt{\frac{kT_e}{2\pi m_e}} \exp\left(\frac{e\Phi_w}{kT_e}\right), \quad (A4)$$

so the ion density becomes

$$\begin{aligned} n_i &= n_e \sqrt{\frac{m_i}{2\pi kT_n}} \frac{n_0}{n_{e,av}} \sqrt{\frac{kT_e}{2\pi m_e}} \exp(\Phi_w) \\ &\times \int \exp\left(1 + \frac{e(\Phi' - \Phi)}{2kT_n}\right) K_0\left(\left|\frac{e(\Phi' - \Phi)}{2kT_n}\right|\right) dx'. \end{aligned} \quad (A5)$$

After inserting the expression $n_e = n_0 \exp(e\Phi/kT_e)$ B&J obtained their famous equation, which in an un-normalized form reads,

$$\frac{1}{B} = \int \exp\left(1 + \frac{e(\Phi' - \Phi)}{2kT_n}\right) K_0\left(\left|\frac{e(\Phi' - \Phi)}{2kT_n}\right|\right) dx', \quad (A6)$$

where, for brevity’s sake, B&J introduced symbol B for a short expression of the eigenvalue of the problem as

$$B = \frac{1}{2\pi} \sqrt{\frac{T_e m_i}{T_n m_e}} \frac{n_0}{n_{av}} \exp\left(\frac{e\Phi_w}{kT_e}\right), \quad (A7)$$

with Φ_w the physical wall boundary. Interchanging the dependent and independent variables yields

$$\begin{aligned} \frac{1}{B} &= \int \Psi(\Phi') \exp\left[\left(1 + \frac{1}{2T_n}\right)(\Phi - \Phi')\right] \\ &\times K_0\left(\left|\frac{\Phi - \Phi'}{2T_n}\right|\right) d\Phi', \end{aligned} \quad (A8)$$

which is a Fredholm-type homogeneous equation of the first kind where $\Psi(\Phi') \equiv -1/E$ is the inverse electric field E . So the electric field is the unknown function to be found with a

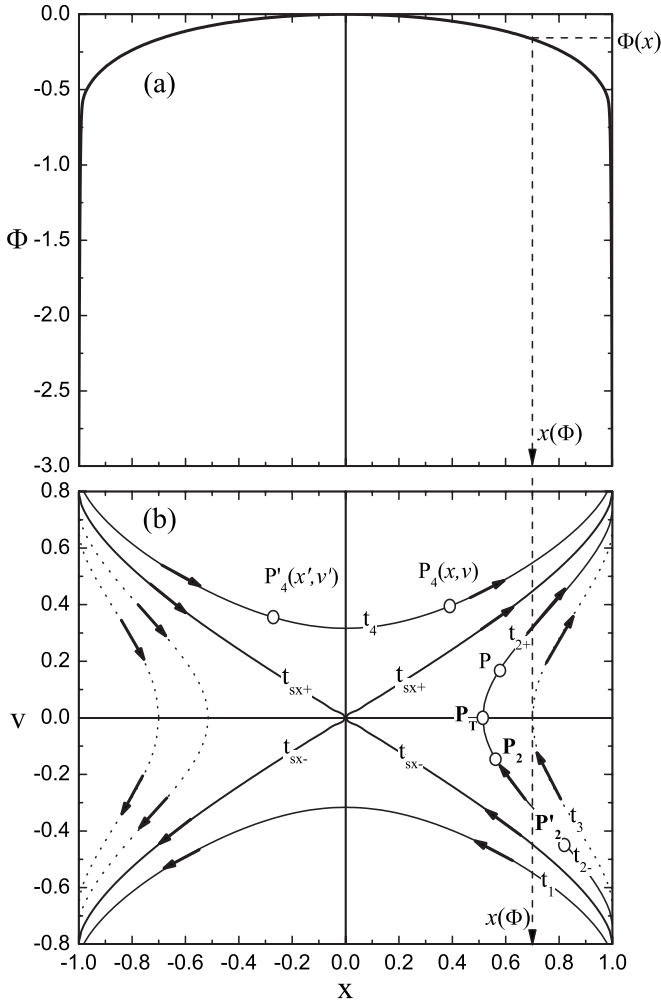


FIG. 12. A randomly chosen potential profile calculated in our PIC simulations (a) with corresponding particle trajectory diagram (b).

known analytic kernel (the rest of integrand which we will refer to as the B&J kernel).

Once a numerical solution of the system (A8) is obtained, it is straightforward (but not easy) to calculate the ion velocity distribution which in normalized variables in accordance to B&J reads

$$f_i[\Phi(x), v] = B \int_{\Phi'} \Psi(\Phi') \exp(\Phi') \times \frac{\exp\{-[v^2 - (\Phi' - \Phi)]/T_i\}}{\sqrt{v^2 - (\Phi' - \Phi)}} d\Phi'. \quad (\text{A9})$$

APPENDIX B: THE TRAJECTORY METHOD

The velocity distribution at any observation point of the discharge for a general ion source up to the wall can be obtained by performing an analysis of the phase space trajectories crossing the observation point from either its right or its left side, based on the energy conservation $v^2 + \Phi = v'^2 + \Phi' = \text{Const}$. Let us now look at Fig. 12(a), where the place of the observation is an arbitrary point, the ion birth places are denoted with prime ('), so an integration of all the birth places should be carried one,

$$f_i(x, v) = \int_{\Phi_{\text{start}}}^{\Phi(x)} \frac{d\Phi'}{-E(\Phi')} \frac{S(x', v')}{v'}. \quad (\text{B1})$$

- (1) First, we look at the trajectories of particles which pass point $x(\Phi)$ from its right to its left side, i.e., the trajectories of the type between t_1 and t_2 (including separatrix t_{sx-} and excluding all the particles of type t_3 and other trajectories with insufficient energy to pass from the right to the left side of the observation point). The contribution of these particles to the ion velocity distribution is thus

$$f_i(x, v) = H(-v) \int_{\Phi_w}^{\Phi(x)} \frac{d\Phi'}{-E(\Phi')} \frac{S(x', v')}{v'}, \quad (\text{B2})$$

where $H(x)$ is the Heaviside step function.

- (2) Second, we look at the particles passing point $x(\Phi)$ from its left to its right, whose place of birth is at the right side of the plane of symmetry between separatrices t_{sx-} and t_{sx+} :

$$f_i(x, v) = [H(v)H(\sqrt{-\Phi} - v)] \times \left[\int_{\Phi_w}^{\Phi(x)+v^2} \frac{d\Phi'}{-E(\Phi')} \frac{S(x', v')}{v'} - \int_{\Phi(x)+v^2}^{\Phi(x)} \frac{d\Phi'}{-E(\Phi')} \frac{S(x', v')}{v'} \right]. \quad (\text{B3})$$

Here the first integral belongs to those ions which are born at either side of point $x(\Phi)$ and have a turning point P_T , i.e., born with negative velocities (the bottom part of the trajectory of type t_2), while the second integral belongs to the ions born with positive velocities (the upper part of the trajectory of type t_2).

- (3) Finally, we look at the particles passing point $x(\Phi)$ from its left to its right side, whose place of birth is above separatrix t_{sx+} (type t_4)

$$f_i(x, v) = [H(v - \sqrt{-\Phi})] \left[\int_{\Phi_w}^0 \frac{d\Phi'}{-E(\Phi')} \frac{S(x', v')}{v'} - \int_0^{\Phi(x)} \frac{d\Phi'}{-E(\Phi')} \frac{S(x', v')}{v'} \right], \quad (\text{B4})$$

where the first integral belongs to those ions which are born at the left hand side of the plane of symmetry (with enough energy to overcome the potential maximum) and the second integral considers those particles which are born with positive velocities in the region between the plane of symmetry and observation point $x(\Phi)$ (no turning point).

Thus we obtain the velocity distribution as a composition of three parts, i.e., for negative velocities, for velocities between 0 and $\sqrt{-\Phi}$, and for those greater than $\sqrt{-\Phi}$. The illustration of the method is shown in Fig. 12(b). With explicit source distribution, which is in this work assumed to be Maxwellian, the nondimensional form of ion VDF is

$$f_i[\Phi(x), v] = B \int_0^1 dx' \exp(\Phi') \frac{\exp\{-[v^2 - (\Phi' - \Phi)]/T_n\}}{\sqrt{v^2 - (\Phi' - \Phi)}}. \quad (\text{B5})$$

The normalized velocity distributions at various points $x(\Phi)$ for the cases of an analytically solved problem of the zero ion source temperature, a very small ion source temperature, and a rather high source temperature $T_{i,\text{src}}=T_e$ were shown in Sec. III. The moments of velocity distribution are fluid quantities, which are obtained as an infinite series of integrals $\int_{-\infty}^{\infty} v^j f_i(v) dv$, where $j=0, 1, 2, \dots$. Such quantities are, e.g., the ion density

$$n_i[\Phi(x)] = \int_{-\infty}^{\infty} f_i(v) dv, \quad (\text{B6})$$

the ion flux

$$\Gamma_i[\Phi(x)] = \int_{-\infty}^{\infty} v f_i(v) dv, \quad (\text{B7})$$

the ion total energy

$$K_i[\Phi(x)] = \frac{1}{n_i(\Phi)} \int_{-\infty}^{\infty} v^2 f_i(v) dv, \quad (\text{B8})$$

and derived quantities like ion directional velocity

$$u_i[\Phi(x)] = \frac{1}{n_i(\Phi)} \Gamma_i(\Phi), \quad (\text{B9})$$

the ion temperature

$$T_i[\Phi(x)] = K_i(\Phi) - u_i^2(\Phi), \quad (\text{B10})$$

as well as all higher moments like heat flux, energy flux, etc. at any location.

APPENDIX C: NUMERICAL METHOD

We can first look for a solution of Eq. (25) without the unknown additive constant ϕ_0 . Once this solution is found, the additive constant is simply calculated from the vertical shift of the solution. Quantity B (related to the source strength) in our algorithm is calculated and iterated at each loop.

We start from Eq. (20) that is discretized over interval $x=[0, 1]$ with a varying density of sample points x_i . For a subsequent purpose of derived quantities like $dx/d\Phi$ a dense grid near zero is needed. The location of the i th position at the grid is given by

$$x_i = \left[1 - \left(1 - \frac{i}{N-1} \right)^{\lambda_2} \right]^{\lambda_1}, \quad (\text{C1})$$

for the index range $i=0, 1, \dots, N-1$, which covers x range of interest for N points. The grid density near zero is controlled via λ_1 , while λ_2 controls the density near $x=1$. Practical values for λ_1 and λ_2 range from 2 to 3 for grids with $N \geq 1000$ points. It should be noted that the grid density approaching $x=1$ is extremely high and that an equivalent interval density can be as high as 10^8 points.

For function $\Phi(x)$ discretized at points x_i and break into $N-1$ intervals piecewise-linear profiles are assumed. The interpolating function $V(x')$ over each interval can be evaluated with

$$V(x') = V_i + \frac{V_{i+1} - V_i}{x_{i+1} - x_i} (x' - x_i), \quad x_i \leq x' \leq x_{i+1}, \quad (\text{C2})$$

where V_i represents discrete function value $V_i = \Phi(x_i)$. In a discrete form Eq. (25) is rewritten into

$$\begin{aligned} & \exp \left[\left(1 + \frac{1}{2T_i} \right) V_k \right] \\ &= B \sum_{i=0}^{N-1} \left\{ \int_{x_i}^{x_{i+1}} dx' \times \exp \left[\left(1 + \frac{1}{2T_n} \right) V(x') \right] \right. \\ & \quad \left. \times K_0 \left(\frac{1}{2T_i} |V_k - V(x')| \right) \right\}. \end{aligned} \quad (\text{C3})$$

The right-hand side of Eq. (C3) can be abbreviated and formulated in the iterative form as

$$V_k = \frac{1}{1 + \frac{1}{2T_n}} \ln \left(B \sum_{i=0}^{N-1} L_i \right), \quad (\text{C4})$$

where L_i represents the integral over each interval that should be evaluated for every index i at position k . A careful investigation of plasma Eq. (C3) that has the property of monotonicity reveals that for each position k there are at the most two neighboring intervals that lead to singularity of the Bessel function. These singular intervals with integrable singularity at the boundary can be numerically solved with adaptive quadrature integration algorithms.^{17,18} The remaining intervals should not impose any numerical difficulties and can be solved with a nonsingular quadrature formula over each interval. Note that this is not completely true and that observing Eq. (C2) one can see that on condition $V_{i+1} - V_i \equiv 0$ additional singularity might arise, if monotonicity is not strictly maintained over the whole interval $[0, 1]$. Especially intervals near zero are prone for such singularities. Another observation of a numerical nature that might arise in Eq. (C2) can be observed with high gradients approaching $x=1$ and dense intervals that can lead to unstable discrete derivative $c_i = (V_{i+1} - V_i)/(x_{i+1} - x_i)$ found in Eq. (C2).

These observations should be carefully considered when integrating Eq. (C3) fully numerically at every k . One can also conclude that the chosen λ_1 and λ_2 as grid parameters have indirect influence on the presence of numerical instabilities and the presence of singularities that should be avoided as much as possible.

The formula (C4) where the right-hand side of equation evaluates to new V_k is mathematically exact, but can only be applied when all V_k are perfectly accurate. With $V_k \rightarrow V_l$ on the left-hand side of Eq. (C4) and additional soft-step parameter α one can get an iterative algorithm for new V_k values with

$$V_k^{\text{new}} = V_k + \alpha(V_l - V_k). \quad (\text{C5})$$

While the method (C5) converges, it does so very slowly. The practical values for α are from 0.0001 to 0.1 and are dependent on the initial solution and grid parameters. Large α 's are prone to oscillatory behavior that starts at points near $x=0$.

To speed up the computation, one can first compute an approximation on a coarser grid and gradually lower α when interpolating to the dense grid. An alternative approach when changing T_i is to start with an already converged solution for nearby T_i . The initial solution is recommended, although not required, to be as close as possible to the final solution. We suggest the following monotonous initialization function

$$V_k = 0.5[1 - \exp(k/N)], \quad k = 0, 1, \dots, N-1, \quad (\text{C6})$$

disregarding λ_1 and λ_2 .

To stabilize the convergence we introduced two additional vanishing *a posteriori* regularization operations on Eq. (C5) that are based on the known solution smoothness. A simple Laplacian-like smoothing technique with smooth-step parameter β similar to Eq. (C5) is employed as

$$V_k^{\text{new}} = V_k + \beta \left[\frac{V_{k-1} + V_{k+1}}{2} - V_k \right], \quad (\text{C7})$$

$$k = N-1, N-2, \dots, 1.$$

Choosing $\beta \leq 1$ stabilizes the convergence and should be gradually lowered to zero when the solution stabilizes. After observing the nature of instabilities, we found out that oscillatory behavior starting at $x=0$ propagates throughout the mesh. To prevent this, we enforced a parabolic interpolation for the first m points that are rewritten with

$$V_k = ax_k^2 + bx_k + c, \quad k = 0, 1, \dots, m, \quad (\text{C8})$$

$$a = \frac{V_l - V_m}{x_l^2 - x_m^2}, \quad b = 0, \quad c = \frac{x_l^2 V_m - x_m^2 V_l}{x_l^2 - x_m^2},$$

where mesh point x_l is chosen at $l=3/4m$. The length of the rewritten profile can be up to $x_m < 0.1$ and gradually lowered when approaching the final solution. Constant B is unknown during the iterative procedure and as shown in Eq. (25) influences the shift of the solution. From Eq. (C3) B can be expressed as

$$B = \frac{\exp\left[\left(1 + \frac{1}{2T_n}\right)V_k\right]}{\sum_{i=0}^{N-1} L_i}, \quad (\text{C9})$$

with V_k being the old value, while L_i 's are next iteration zone integrals. Constant B should hold at every grid point. As an eigenvalue, B does not have a major impact on convergence. Similarly to other smooth step parameters, B should also be adjusted with soft step of 0.005, calculated from the central grid point. Our experiments showed that initial $B=0.3$ can be used for all cases.

The iterative process can be summarized through the following steps.

(1) Setup B and grid positions using Eq. (C1).

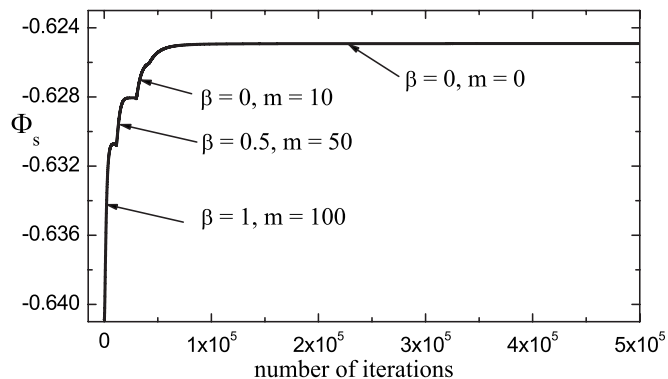


FIG. 13. Convergence for $T_n=1$ with gradually lowering smooth step and parabolic rewrite took about 500 000 iterations and nearly 1 week of 8 core Intel Xeon 2 GHz processor time.

- (2) Create the initial solution with Eq. (C6) or initialize the function profile with the nearest previous solution, if existent.
- (3) For every grid position calculate the sum of integrals V_k using Eq. (C4).
- (4) Move function values V_k into a new position with a soft-step strategy (C5) using step size α in the range $[0.0001, 0.1]$.
- (5) Stabilize the convergence with additional smoothing of the curve with Eq. (C7) that prevents the oscillatory behavior of the solution. Similarly to Eq. (C5), the step size should vanish as the solution approaches the stable form.
- (6) Prevent oscillations near $x=0$ with a parabolic rewrite of the potential profile for all points with $x_m < 0.1$. Use Eq. (C8) for the coefficients of the parabolic interpolation.
- (7) Calculate B using Eq. (C9) and correct its value for 0.005 of the difference between new and old B .
- (8) Repeat the iteration from step 3 following the solution quality criterions while gradually lowering the smooth step and the parabolic interpolation range.

The stopping criteria for the iteration procedure cannot be simply expressed with a measure like the quadrature norm between the iterations. One of the most important convergence indicators is a potential at $x=1$. During the convergence one should observe the curve properties near $x=0$, where the parabolic interpolation ends. Potential V_{N-1} at $x=1$ can also behave oscillatorily, with a convergent amplitude. The number of iteration steps depends on a number of factors and can range from 2000 to 100 000. The most influential is the soft-step size that should be as high as possible. Setting the soft step too high produces undesirable oscillations at the beginning of the potential curve that cannot be easily rescued once they appear. The strategy for lowering smooth-step β and the parabolic interpolation is that, first, one should have a convergent solution and then smoothly lowering both parameters that should vanish for the final solution. Figure 13 shows the described scenario with both parameters lowered, while monitoring the convergence, i.e., without the oscillatory nature through all computational area. The implementation of the described approach was verified and coded in MATHEMATICA and the C language using the

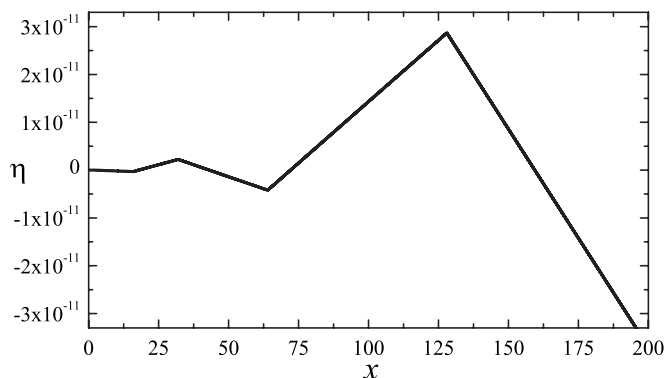


FIG. 14. Relative error η of the Bessel function $K_0(x)$ in the GLS library for double precision used in our approach shows relative error $\eta < 10^{-10}$ in a wide range of the arbitrary argument x .

Gnu Scientific Library (GSL) for special functions and integrations. Most notable here is the Bessel K_0 function with a relative error under $\eta < 10^{-10}$ in a wide range as shown in Fig. 14. The upper limit for double machine precision K_0 obtained with this experiment is approximately 600, which is an imposed limit of our code in C on commodity computer architectures. For the numerical integration in zones we used QAG and QAGS quadrature algorithms that adaptively bisects integration into subintervals until the given relative error limit is achieved. The integration of nonsingular zones applies the Gauss–Kronrod 21-point integration rule while for singular zones results are extrapolated using the epsilon algorithm. For more details consult Ref. 19.

While MATHEMATICA was our first choice to prove some convergence experiments, it was soon clear that the problem would be time consuming and that C code would require parallelization for reasonable proof of concept. The number of integral evaluations is directly connected to the number of grid points N . We estimate a practical limit for MATHEMATICA up to 200 points. Our C code with the shared memory model parallelization using OpenMP does not seem to be practically time bound with a number of intervals, but rather with precision limits that are imposed with numeric model and machine precision. For the numeric model we used long double precision wherever possible. The practical number of points that enabled us to derive results was 1600.

The required extremely high refinements at both sides of

the domain are also sources of instabilities that need a special treatment with regard to precision. One must take care that the overall precision of the zone integration results within the high grid density is not violated. The relative error for QAG and QAGS algorithms was set to 10^{-6} with a maximum number 20 000 of workspace for adaptive subintervals.

In our code, we implemented result caching mechanism that enabled us to experiment with parameters, so we could rollback in the presence of instabilities. Once one case is evaluated it is relatively easy to move to the nearby temperature. Depending on solution criteria, computational time on 8 core dual Xeon 2 GHz processor can range from 1h to 1 week. A helpful time-saving approach can be regrid from/to low/high grid density.

- ¹L. Tonks and I. Langmuir, *Phys. Rev.* **34**, 876 (1929).
- ²R. C. Bissell and P. C. Johnson, *Phys. Fluids* **30**, 779 (1987).
- ³J. T. Scheuer and G. A. Emmert, *Phys. Fluids* **31**, 3645 (1988).
- ⁴P. C. Stangeby, *The Plasma Boundary of Magnetic Fusion Devices* (Institute of Physics, Bristol, 2000).
- ⁵K.-U. Riemann, *Phys. Plasmas* **13**, 063508 (2006).
- ⁶A. Caruso and A. Cavaliere, *Nuovo Cimento* (1955–1965) **26**, 1389 (1962).
- ⁷E. R. Harrison and W. B. Thompson, *Proc. Phys. Soc. London* **74**, 145 (1959).
- ⁸M. Abramovitz and I. A. Stegun, *Handbook of Mathematical Functions with Formulas, Graphs and Mathematical Tables* (Dover, New York, 1972), p. 379.
- ⁹C. K. Birdsall and B. A. Langdon, *Plasma Physics Via Computer Simulation* (McGraw-Hill, New York, 1985).
- ¹⁰J. P. Verboncoeur, M. V. Alves, V. Vahedi, and C. K. Birdsall, *J. Comput. Phys.* **104**, 321 (1993).
- ¹¹D. Tskhakaya, S. Kuhn, Y. Tomita, K. Matyash, R. Schneider, and F. Taccogna, *Contrib. Plasma Phys.* **48**, 121 (2008).
- ¹²K.-U. Riemann, private communication (2009).
- ¹³S. A. Self, *Phys. Fluids* **6**, 1762 (1963).
- ¹⁴S. Kuhn, K.-U. Riemann, N. Jelić, D. D. Tskhakaya, Sr., D. Tskhakaya, Jr., and M. Stanojević, *Phys. Plasmas* **13**, 013503 (2006).
- ¹⁵N. Jelić, K.-U. Riemann, T. Gyergyek, S. Kuhn, M. Stanojević, and J. Duhovnik, *Phys. Plasmas* **14**, 103506 (2007).
- ¹⁶ASDEX Upgrade Team, A. V. Chankin, D. P. Coster, R. Dux, C. Fuchs, G. Haas, A. Herrmann, L. D. Horton, A. Kallenbach, M. Kaufmann, A. S. Kukushkin, K. Lackner, H. W. Müller, J. Feuhauser, R. Pugno, and M. Tsallas, *J. Nucl. Mater.* **363–365**, 335 (2007).
- ¹⁷P. Favati, G. Lotti, G. Di Marco, and F. Romani, *J. Complex.* **10**, 296 (1994).
- ¹⁸P. Favati, G. Lotti, and F. Romani, *ACM Trans. Math. Softw.* **17**, 218 (1991).
- ¹⁹R. Piessens, E. de Doncker-Kapenga, C. W. Uberhuber, and D. K. Kahaner, *Quadpack. A Subroutine Package for Automatic Integration*, Series in Computational Mathematics 1 (Springer-Verlag, Berlin, 1983).